Received January 2002
Revised February 2003
Accepted April 2003

Aeroelastic analysis of turbomachinery

Part II – stability computations

R. Srivastava, M.A. Bakhle and T.G. Keith Jr
The University of Toledo, Toledo, Ohio, USA
D. Hoyniak
Rolls-Royce, Indianapolis, Indiana, USA

Keywords *Fourier analysis, Time series analysis, Multiple time series, Aircraft engines*

Abstract *Part II of the two-part paper describes an aeroelastic analysis program and its application for stability computations of turbomachinery blade rows. Unsteady Euler or Navier-Stokes equations are solved on dynamically deforming, body fitted, and grid to obtain the aeroelastic characteristics. Blade structural response is modeled using a modal representation of the blade and the work-per-cycle method is used to evaluate the stability characteristics. Non-zero inter-blade phase angle is modeled using phase-lagged boundary conditions. Results are presented for a flat plate helical fan, a turbine cascade and a high-speed fan, to highlight the aeroelastic analysis method, and its capability and accuracy. Obtained results showed good correlation with existing experimental, analytical and numerical results. Numerical analysis also showed that given the computational resources available currently, engineering solutions with good accuracy are possible using higher fidelity analyses.*

Introduction

Numerical methods for the prediction of aeroelastic stability characteristics of turbomachines with various degrees of fidelity are being used regularly for the design and analysis of turbomachinery blade rows. Methods based on energy exchange between vibrating blades and surrounding fluid, have been reported using semi-analytical methods (Lane and Friedman, 1958; Smith, 1972), linearized Euler method (Verdon, 1993), Euler methods (Bakhle *et al.*, 1997; Gerolymos and Vallet, 1994; He, 1989), linearized viscous method (Clark and Hall, 2000), and viscous methods (Giles and Haimes, 1991; He and Denton, 1994; Marshall *et al.*, 2000; Siden, 1991). A limited number of coupled aeroelastic analyses of turbomachine configurations have also been reported (Breard *et al.*, 2000; Gerolymos, 1992; Srivastava and Reddy, 1999; Williams *et al.*, 1991). Williams *et al.* (1991) used a linear panel method to solve the eigenvalue problem. Gerolymos (1992) and Srivastava and Reddy (1999) solved the coupled aeroelastic equations based on an inviscid aerodynamic analysis.

International Journal of Numerical Methods for Heat & Fluid Flow
Vol. 14 No. 3, 2004
pp. 382-402

0961-5539
DOI 10.1108/09615530410518011

This work was supported by the Advanced Subsonic Technology and the Ultra Efficient Engine Technology projects through a grant from NASA Glenn Research Center.

Recently, Breard, *et al.* (2000) solved the coupled aeroelastic equations using Navier-Stokes equations to calculate the forced response of fan blades due to inlet distortions.

The objective of the present effort is to report an aeroelastic analysis program based on Euler/Navier-Stokes equations and its application to turbomachinery blade rows. The results obtained are compared to those obtained from a two-dimensional linear method which solves the linear, compressible, potential flow equation (Smith, 1972), to those obtained from a two-dimensional linearized viscous analysis (Clark, 1998), and to the existing experimental data from a linear turbine blade cascade (Rothrock *et al.*, 1981) and a transonic fan configuration (Fite, 2001).

The TURBO-AE code

The aeroelastic solver TURBO-AE is briefly described in this section. The solver can model multiple blade rows undergoing harmonic oscillations with arbitrary inter-blade phase angles (IBPAs). It is based on a Euler/Navier-Stokes unsteady aerodynamic solver for internal flow calculations of axial flow turbomachinery components TURBO (Chen, 1991; Janus, 1989). Good comparisons with the experimental data for steady and unsteady aerodynamic analyses have been reported using the TURBO code (Barter *et al.*, 2000; Chen and Barter, 1998). Navier-Stokes equation in conservation form can be written as

$$\frac{\partial \mathbf{q}}{\partial t} + \frac{\partial(\mathbf{E} - \mathbf{E}_v)}{\partial x} + \frac{\partial(\mathbf{F} - \mathbf{F}_v)}{\partial y} + \frac{\partial(\mathbf{G} - \mathbf{G}_v)}{\partial z} = 0 \tag{1}$$

where $\mathbf{q}$ is the vector of unknown flow variables in conservation form

$$\mathbf{q} = \begin{Bmatrix} \rho \\ \rho u \\ \rho v \\ \rho w \\ e \end{Bmatrix}$$

with

$$\mathbf{E} = \begin{Bmatrix} \rho u \\ \rho u^2 + p \\ \rho uv \\ \rho uw \\ u(e+p) \end{Bmatrix} \quad \mathbf{F} = \begin{Bmatrix} \rho v \\ \rho uv \\ \rho v^2 + p \\ \rho vw \\ v(e+p) \end{Bmatrix} \quad \mathbf{G} = \begin{Bmatrix} \rho w \\ \rho uw \\ \rho wv \\ \rho w^2 + p \\ w(e+p) \end{Bmatrix}$$

$$\mathbf{E}_{\mathrm{v}} = \begin{Bmatrix} 0 \\ \tau_{xx} \\ \tau_{xy} \\ \tau_{xz} \\ Q_x \end{Bmatrix} \quad \mathbf{F}_{\mathrm{v}} = \begin{Bmatrix} 0 \\ \tau_{yx} \\ \tau_{yy} \\ \tau_{yz} \\ Qy \end{Bmatrix} \quad \mathbf{G}_{\mathrm{v}} = \begin{Bmatrix} 0 \\ \tau_{zx} \\ \tau_{zy} \\ \tau_{zz} \\ Q_z \end{Bmatrix}$$

and

$$Q_x = u\tau_{xx} + v\tau_{xy} + w\tau_{xz} - \hat{q}_x$$
$$Q_y = u\tau_{yx} + v\tau_{yy} + w\tau_{yz} - \hat{q}_y$$
$$Q_z = u\tau_{zx} + v\tau_{zy} + w\tau_{zz} - \hat{q}_z$$

where ρ is the fluid density, u, v, and w are the Cartesian velocity components, e is the total internal energy, and x, y, z are Cartesian coordinates. Variables **E**, **F**, and **G** are inviscid flux vectors, $\mathbf{E}_{\mathrm{v}}$, $\mathbf{F}_{\mathrm{v}}$, $\mathbf{G}z_{\mathrm{v}}$ are viscous flux vectors, $\hat{q}_x, \hat{q}_y, \hat{q}_z$ are heat fluxes, and $\tau_{xx}, \tau_{xy}, \tau_{zy}$ etc. are stress vectors. Two-equation k-ε turbulence model is used for closure (Shih *et al.*, 1995).

Representing Navier-Stokes equations in the form shown in equation (1) has the advantage that by setting the viscous flux vectors to zero, the solver becomes an Euler solver. To simplify treatments of arbitrary geometries, Navier-Stokes equation in (1) are transformed and recast in a generalized body-fitted coordinate system. The transformed equations are solved using a finite volume scheme. Flux vector splitting is used to evaluate the flux Jacobians on the left-hand side. The right-hand side fluxes are discretized using high order total variation diminishing (TVD) scheme based on Roe's flux difference splitting. Newton subiterations are used at each time-step to find an approximate solution to the nonlinear finite volume discretization. Symmetric Gauss-Seidel relaxations are applied to solve the resulting linear system.

Aeroelastic analysis

Aeroelastic characteristics of the rotor are obtained by calculating the energy exchange between the vibrating blade and its surrounding fluid. If work on the blade is positive, it indicates instability. The aeroelastic analysis is carried out first by obtaining the "steady" aerodynamic solution for a given operating condition. The blades are then forced into a prescribed harmonic motion (specified mode, frequency, and IBPA) to calculate the unsteady aerodynamic response and work-per-cycle. The blade motion is simulated using a dynamic grid deformation technique. For a harmonic motion in a selected normal mode, the displacement of any point on the blade $\vec{X}(x, y, z, t)$ can be written in terms of the generalized coordinate $q(t)$ and the modal deflection $\vec{\delta}(x, y, z)$ as

$$\vec{X}(x, y, z, t) = q(t)\vec{\delta}(x, y, z) \tag{2}$$

For a prescribed harmonic motion

$$q(t) = q_0 \sin(\omega t) \tag{3}$$

with amplitude of motion q_0 and vibration frequency ω, the work-per-cycle can be calculated as

$$W = \oint \int_{\text{surface}} p \cdot \mathrm{d}\vec{\mathrm{A}} \bullet \left(\frac{\partial \vec{X}}{\partial t}\right) \mathrm{d}t \tag{4}$$

using equations (2) and (3), the work-per-cycle can be rewritten as

$$W = \oint \int_{\text{surface}} p \cdot \mathrm{d}\vec{\mathrm{A}} \bullet \vec{\delta} \mathrm{q}_0 \omega \cos(\omega t) \mathrm{d}t \tag{5}$$

where p is the blade surface pressure and $\vec{\mathrm{A}}$ is the surface area vector. The aerodynamic damping associated with the blade motion can then be calculated by taking the ratio of work-per-cycle with the associated kinetic energy of the blade (Carta, 1967):

$$\frac{W}{K_{\mathrm{E}}} = -\frac{8\pi\gamma}{\sqrt{1-\gamma^2}} \tag{6}$$

here γ is the damping ratio and K_{E} is the kinetic energy of the blade, defined as

$$\gamma = \frac{C}{C_{\mathrm{cr}}} \tag{7}$$

$$C_{\mathrm{cr}} = 2m\omega \tag{8}$$

$$K_E = \frac{1}{2} m V^2 \tag{9}$$

with C being the damping and C_{cr} the critical damping, m is the mass of the blade and V is the surface velocity due to blade vibration.

For small values of γ

$$\sqrt{1 - \gamma^2} \approx 1 \tag{10}$$

Using equation (10) in equation (6), the damping ratio can be calculated as

$$\gamma = -\frac{W}{8\pi K_E} \tag{11}$$

The work-per-cycle W is calculated using the TURBO-AE code for a prescribed frequency, IBPA, and mode shape. Using the work-per-cycle, the damping of the system is calculated as a post-processing. To eliminate the need of modeling multiple blade passages, phase-lagged boundary conditions are used to calculate the non-zero IBPA vibrations.

Results and discussion

Results were obtained for a flat plate helical fan, a linear cascade of turbine blades and a transonic fan configuration. These results are compared with the existing analytical, numerical or experimental data.

Flat plate helical fan

The helical fan geometry consists of 24 unswept, untapered, zero thickness, twisted flat plate blades enclosed within a rigid cylindrical duct of infinite length with no tip gap. The fan's operating condition was set at a relative inflow Mach number of 0.7 and zero incidence at midspan with a 0.495 axial Mach number.

Linear turbine cascade

A cascade of turbine blades with large flow turning (112°) was tested for several expansion ratios, exit Mach numbers and IBPAs (Rothrock *et al.*, 1981). The experimental facility consisted of a cascade comprising of five airfoil sections in a stator configuration. In TURBO-AE the linear cascade was modeled as an annular cascade with 96 blades, with a 0.98 hub-tip-ratio, and a tip radius of 21.4625 in. These parameters were selected to match the solidity of the test cascade at midchord. The analysis was carried out for two measured conditions (Table I):

(1) 1.531 expansion ratio with exit flow Mach number of 0.78, and

(2) 2.731 expansion ratio with exit flow Mach number of 1.25.

Transonic fan

A scale model of an experimental transonic fan with 22 blades, design rpm of 15,444, relative tip Mach number of 1.4, and mass flow of 44.85 kg/s was tested in a rig. The fan fluttered at part speed in the first bending mode (Fite, 2001). Results are presented for 90 percent speed at several back pressures and IBPAs.

Flat plate helical fan

Results obtained for the flat plate helical fan configuration and an inviscid analysis using TURBO-AE are presented in this section. The advantage of this configuration and flow condition is that the flow is subsonic and well behaved, and a large hub to tip ratio allows modeling a two-dimensional (2D) flowfield that can be closely approximated at the midspan of the blade. This allows a comparison with the results obtained from an analytical solution using linear theory (Smith, 1972). Montgomery and Verdon (1997) using a linearized Euler analysis have also analyzed this particular configuration.

The configuration with flat plate of zero thickness at zero incidence will have no steady load on the blade. The comparison of the unsteady pressure difference with results obtained by Montgomery and Verdon (1997) for 0° IBPA for pitching and 180° IBPA for plunging motion are shown in the work of Srivastava *et al.* (2004). Figure 1 shows the unsteady moment variation with phase angle for the pitching motion. The unsteady lift variation with phase angle for the plunging motion is shown in Figure 2. The results obtained from TURBO-AE are compared with the results obtained from the linear theory (Smith, 1972) in these figures. Good agreement is obtained for over most of the range except in the neighborhood of acoustic resonance (cut-on and cut-off regions).

The acoustic resonance occurs at phase angles of 107.3 and 330.6°; these values are marked on the phase angle axis of the figures for reference. The phase angles between these resonances are associated with subresonant (Verdon, 1989) (cut-off) conditions in which all disturbances attenuate away from the cascade. No disturbances propagate upstream or downstream under subresonant conditions. The phase angles between 0 and 107.3° and between 330.6 and 360° are associated with super-resonant (cut-on) conditions in which at least one disturbance propagates in either the far upstream or downstream

Ideal inlet total to exit static expansion ratio	Mass averaged expansion ratio	Inlet Mach number	Inlet static pressure ratio	Cascade incidence angle	Mass averaged exit Mach number
1.5:1	1.531	0.5	12.74	−6.6	0.78
2.8:1	2.731	0.52	12.30	−6.6	1.25

Table I.
Turbine cascade test conditions

direction. Figure 2 shows the unsteady lift for plunging blade motion. As noted for the pitching results, these results are also from midspan location and were calculated using the first harmonic of the unsteady blade surface pressure difference. Results from linear potential theory (Smith, 1972) are included in Figure 2 for comparison. The overall level of agreement with linear theory is good. Deviations are observed close to the acoustic resonances, as for pitching. The level of agreement is better for pitching motion than plunging motion.

Figure 3 shows the variation of the unsteady pressure difference with chord for several phase angles for the pitching motion. The variation for the plunging motion is shown in Figure 4. These results are for the first harmonic of the unsteady blade surface pressure difference at the midspan location. The results obtained are compared with the results from the linear theory (Smith, 1972) in these figures. Good agreement is obtained for over most of the range except in the neighborhood of acoustic resonance (cut-on and cut-off regions).

Turbine cascade

The code was applied next to the turbine cascade configuration. A grid size of $129 \times 9 \times 33$ was used to model the blade passage. This section presents the

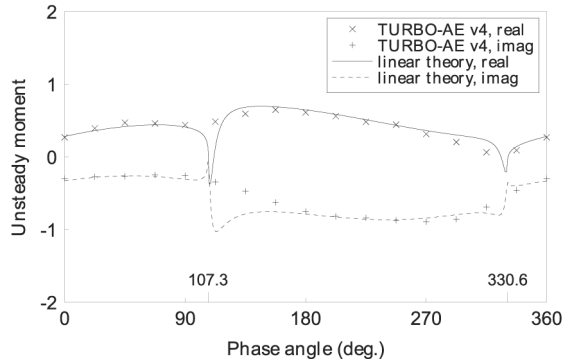

Figure 1.
Unsteady moment variation with IBPA for pitching motion at midchord for $M_\infty = 0.7$

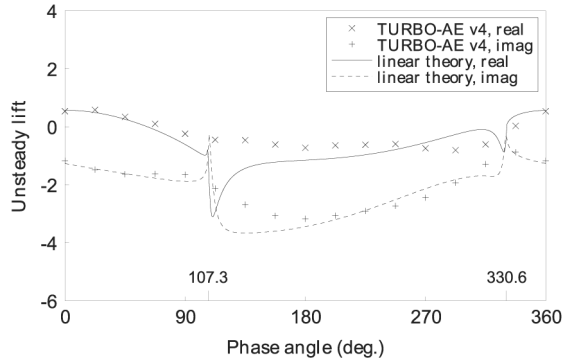

Figure 2.
Unsteady lift variation with IBPA for plunging motion at midchord for $M_\infty = 0.7$

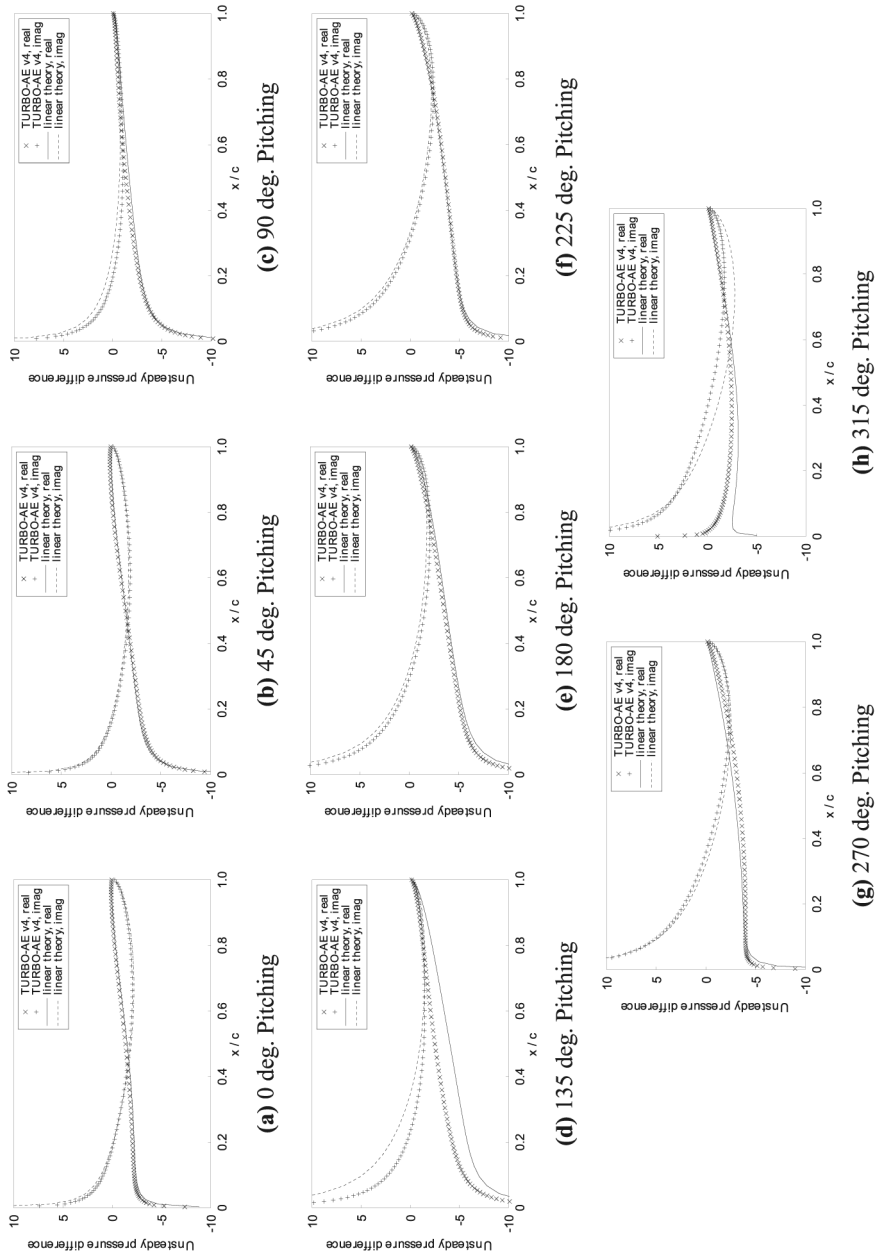

Figure 3.
Unsteady pressure difference (first harmonic) for pitching motion

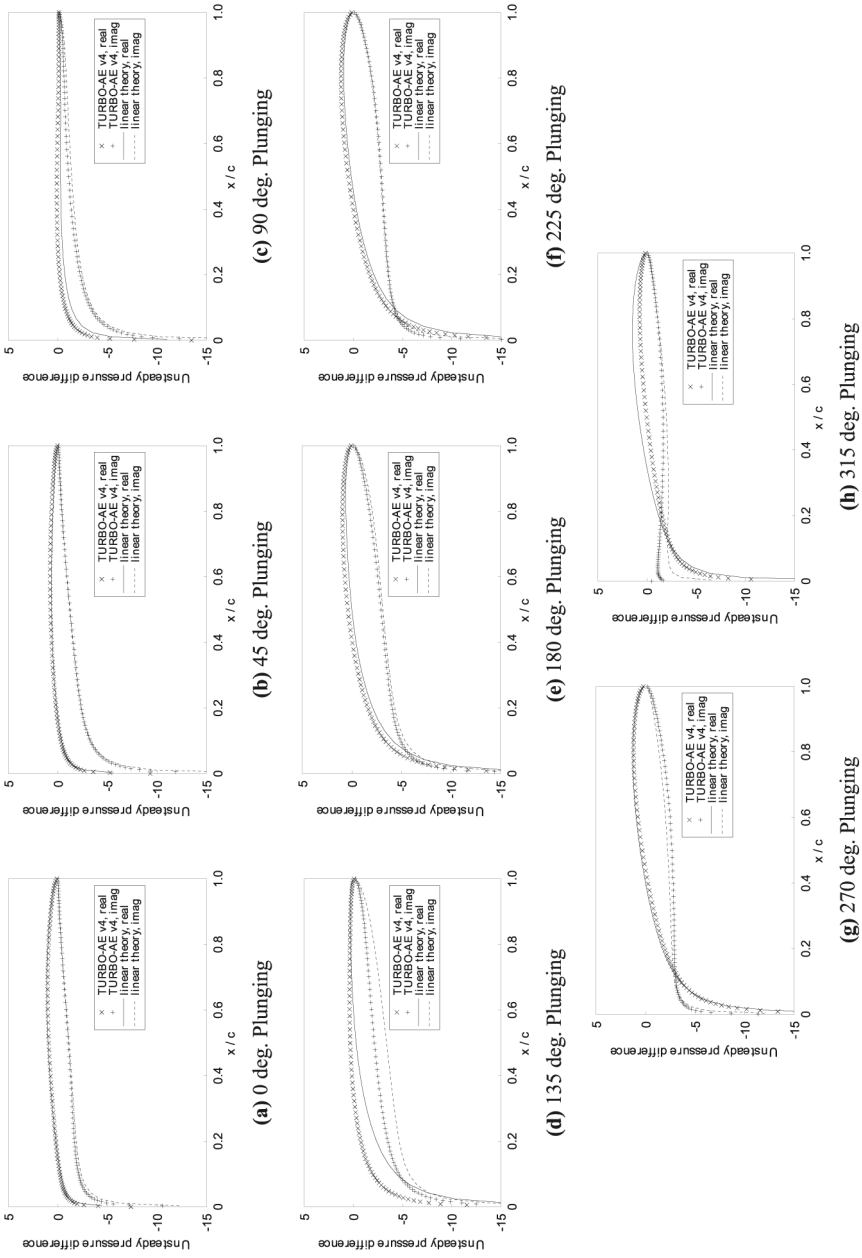

Figure 4.
Unsteady pressure difference (first harmonic) for plunging motion

results of the steady and unsteady predictions for two expansion ratios. The 1.531 expansion ratio corresponds to a case in which the steady flow through the cascade is completely subsonic. The 2.713 expansion ratio provided a test case in which the cascade inlet velocity was subsonic, while the exit velocity was supersonic. A summary of the steady operating conditions considered is given in Table I.

1.531 Expansion ratio

The steady-state pressure variation with chord at midspan for the 1.531 expansion ratio, obtained from TURBO-AE is shown in Figure 5. It also shows the experimental data (Rothrock *et al.*, 1981) and the results from a linearized two-dimensional viscous analysis, LNS2D (Srivastava and Reddy, 1999). Good agreement is obtained with the measured data and the analysis except in a small region on the pressure surface near the leading edge. Evidence obtained during the experimental program indicates that due to the negative incidence angle the flow was separated in this region (Rothrock *et al.*, 1981).

The unsteady response for both expansion ratios was obtained from a torsional motion of the cascade airfoils at 340 Hz and a prescribed IBPA. The TURBO-AE predictions are compared to the measurements and to those obtained from a linearized viscous analysis code LNS2D in Figures 6 and 7 for IBPAs of 0 and 180°, respectively. The TURBO-AE predictions on the suction surface indicate that the unsteady pressure magnitude is being under-predicted over the first 60 percent of the blade. The trend-wise behavior however, compares well with the measurements. The pressure side predictions show a large difference when compared with measurements in the separated region as would be expected for an inviscid analysis. Over the last 40 percent of the pressure side, the predictions compare well to the measurements and the LNS2D analysis. Since the unsteady pressure transducer located at the 30 percent chord position was not operational, no trend information can be inferred over the midsection of the blade. As such it is difficult to assess how

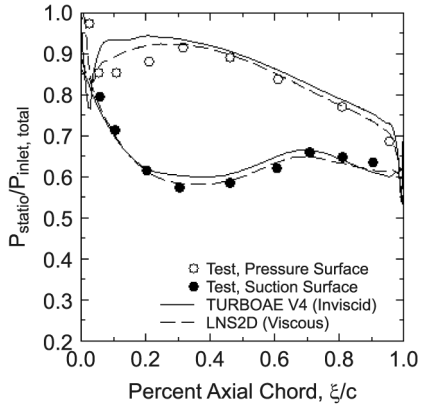

Figure 5.
Comparison of steady blade loading predicted by TURBO-AE and LNS2D with the experimental data

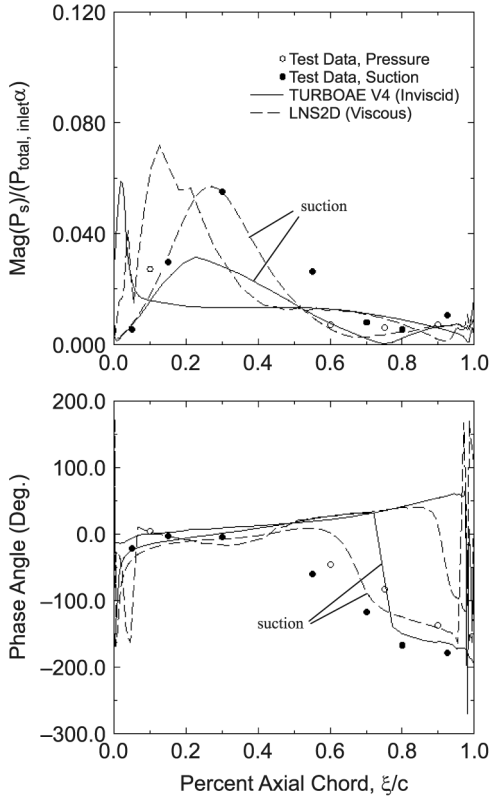

Figure 6.
Comparison of measured and predicted unsteady pressure response for the turbine cascade vibrating in a torsional mode at 340 Hz, 0° IBPA, and 1.531 expansion ratio

well the predictions are doing in this region of the pressure surface. The phase predictions for TURBO-AE for the 0° IBPA case (Figure 6) show good agreement with measurements and LNS2D on the suction surface, but poor agreement with the measurements aft of the midchord on the pressure surface. The phase predictions for the 180° IBPA (Figure 7) show good trendwise agreement with the data. The TURBO-AE phase predictions again show good agreement with the trend of the measurements, but poor agreement with the level of the measurements.

2.713 Expansion ratio

The second steady flow condition studied represented a situation in which the exit flow Mach number became supersonic. In this case the cascade expansion ratio was raised to 2.713. The inlet Mach number became 0.52 and the exit Mach number 1.25 (Table I). Predictions for the steady blade surface pressure distribution obtained from TURBO-AE are compared to the measurements and the LNS2D in Figure 8. Excellent agreement with the measured values and

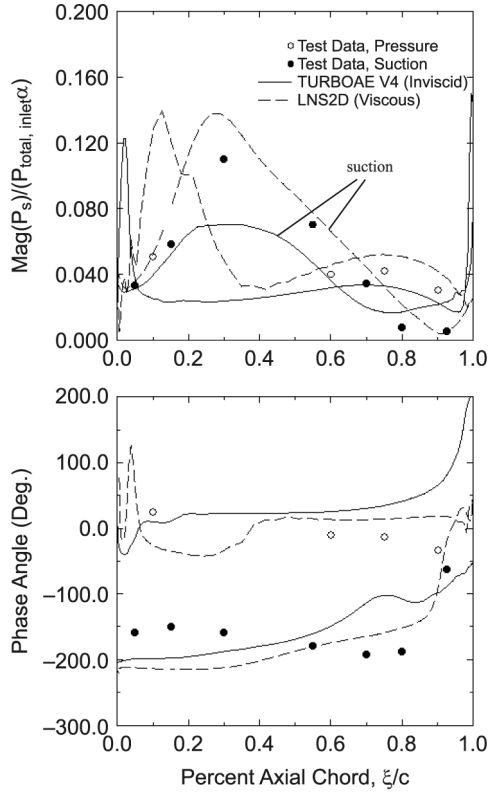

Figure 7.
Comparison of unsteady pressure response for the turbine cascade vibrating in a torsional mode at 340 Hz, 180° IBPA, and 1.531 expansion ratio

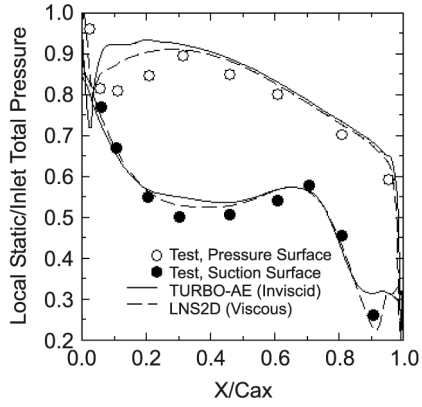

Figure 8.
Comparison of steady blade loading for the 2.713 expansion ratio

LNS2D is obtained over most of the blade surface. The exception is in the leading edge region on the pressure surface where separation occurred. The inviscid results from TURBO-AE would not be expected to match the steady data in this region.

Unsteady predictions obtained from TURBO-AE, for the unsteady blade surface pressure for 0 and 180° IBPAs are compared to the measurements and LNS2D shown in Figures 9 and 10, respectively. The 0° IBPA results (Figure 9) indicate that the TURBO-AE under-predicts the magnitude of the unsteady response on the suction surface. While on the pressure surface, good agreement between prediction and measurement is established aft of midchord. However, over the front half of the blade, both codes predict quite different behaviour. The LNS2D predictions show a maximum in the unsteady magnitude at about the 28 percent chord position. The TURBO-AE predictions, while showing the same level in the unsteady magnitude, indicate that the maximum is achieved at about 2 percent chord. As pointed out earlier, the flow is separated over the first 30 percent of the suction surface, and the unsteady pressure measurements were sparse since a transducer located at the 30 percent chord location was not working. In the trailing edge region of the suction surface, both codes missed the measured increase in unsteady pressure magnitude aft of the point where the trailing edge shock intersects the blade.

Unsteady phase angle predictions from TURBO-AE are also shown in Figures 9 and 10. In this the predictions are in good agreement with the

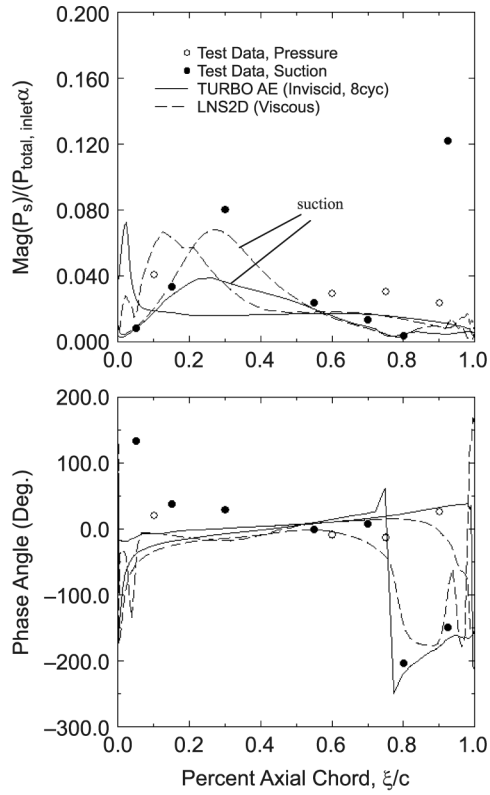

Figure 9.
Comparison of pressure response for the turbine cascade vibrating in a torsional mode at 340 Hz, 0° IBPA, and 2.713 expansion ratio

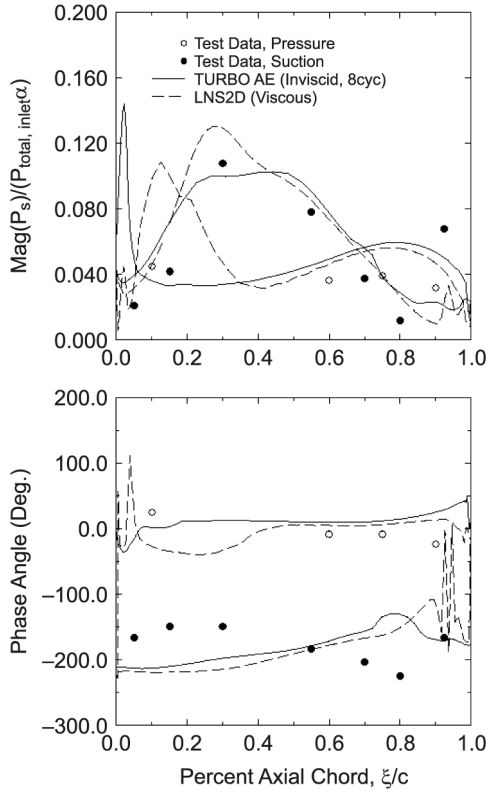

Figure 10.
Comparison of unsteady pressure response for the turbine cascade vibrating in a torsional mode at 340 Hz, 180° IBPA, and 2.713 expansion ratio

measured data. The exception to this observation is in the leading edge region of the suction surface where the measurements differ from both predictions by as much as 150°.

Aerodynamic damping

Unsteady pressure predictions for both expansion ratios were used to calculate the unsteady work-per-cycle as a result of the torsional motion of the blade. When the work being done on the airfoil over one vibration period is positive, the cascade has negative aerodynamic damping and is considered aerodynamically unstable. Figure 11 shows the resulting estimates for the aerodynamic work-per-cycle as a function of IBPA. A very good comparison is obtained between the two analyses. As determined numerically for the higher expansion ratio case, torsional motion of the cascade for this frequency is unstable over a range of IBPAs approximately between 0 and 90°. The lower expansion ratio case was determined to be unstable between 0 and 50°. The inflection point in the low pressure ratio curve in the vicinity of 55° is the result of the calculation being performed near an acoustic resonance point associated with the exit Mach number. No work-per-cycle calculations based on the

measured data have been included in Figure 11, because none were reported at the time that the measurements were made, and it was felt that due to the lack of data on the pressure surface any attempt to integrate the measured pressures to obtain work-per-cycle values would not be accurate. One interesting result shown in Figure 11 is that both expansion ratios exhibit very similar stability characteristics even though their steady loading differs substantially over the aft 20 percent of the suction surface due to the presence of trailing edge shock in the high expansion ratio case. This is due to the relatively weak influence of the unsteady shock loading for this mode shape and flow configuration.

Transonic fan

The analysis was next applied to calculate the aeroelastic characteristics of the transonic fan. The results presented here are for the 90 percent speed line. Experiments showed blade flutter in the first natural mode (natural frequency 351 Hz) for 32.73 IBPA (two nodal diameter forward travelling wave) (Fite, 2001). The calculated time history of mass flow is shown in Figure 12 for

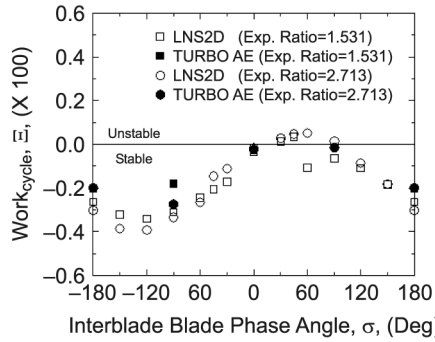

Figure 11.
Unsteady aerodynamic work-per-cycle prediction for turbine cascade, 1.531 and 2.713 expansion ratios

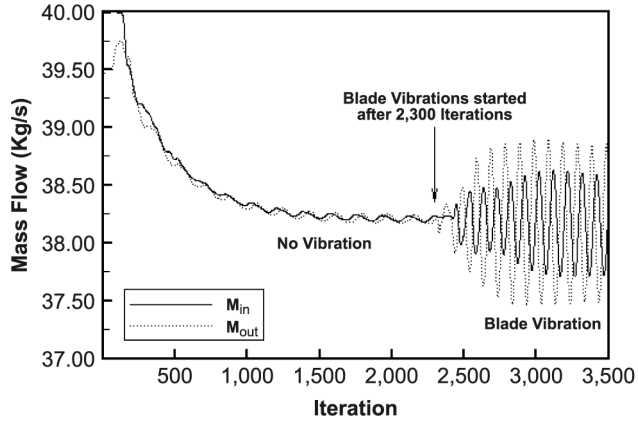

Figure 12.
Variation of mass flow for the transonic fan, with and without blade vibration

flow with and without blade vibration for back pressure of 16.2 psi. The "steady" flow results or results for no blade vibrations show a time dependency, although the mean mass flow is constant. A closer examination of the flowfield revealed flow separation and subsequent shedding of the vortex in the vicinity of the hub in the aft section of the blade. Increasing the back pressure lengthened the region of separation and also moved it further upstream. Figure 12 also shows the variation of mass flow after the blades are forced to undergo prescribed vibration of 180° IBPA at 351 Hz. Because of the mean flow unsteadiness, one needs to ensure that the blade vibration amplitude is large enough so as to minimize the impact of mean flow unsteadiness on the unsteadiness due to blade vibrations. It can be seen from Figure 12 that for the vibration amplitude chosen for the analysis, the unsteadiness due to blade vibration is at least an order of magnitude larger than the mean flow unsteadiness. It can also be seen that the flow converges to periodicity in roughly ten blade vibration cycles.

Figure 13 shows the aerodynamic damping calculated for several different back pressures and IBPAs. For lower back pressures, the least stable IBPA was found to be 0°. However, as the back pressure was raised moving the fan operating condition towards the stall line, the 32.73° IBPA (two nodal diameter forward travelling wave) became least stable. Flutter was observed in the wind tunnel for 32.73° IBPA. The calculated variation of aerodynamic damping with back pressure is shown in Figure 14 for 32.73° IBPA. Figure 14 shows that, as the back pressure is increased, the aerodynamic damping decreases rapidly, dropping to approximately 0.2 percent of critical damping for the back pressure of 16.4 psi. For the grid used, and because of computational constraints, the highest back pressure analyzed was 16.4 psi. Increasing the back pressure above 16.4 psi for 90 percent speed resulted in stalled flow with large separation on the suction surface in the midsection of the blade.

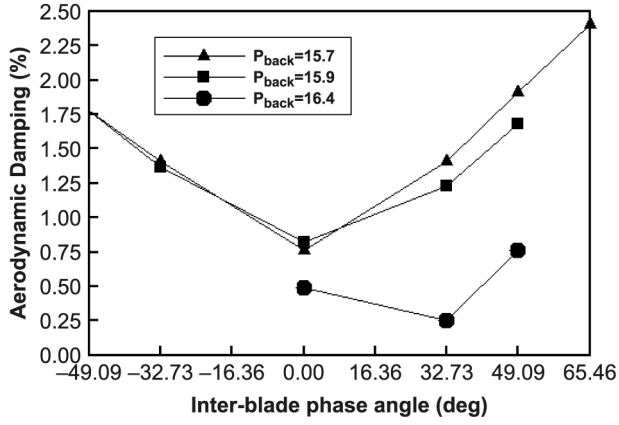

Figure 13.
Variation of aerodynamic damping with back pressure and IBPA for the transonic fan with forced blade vibration in the first natural mode at the natural frequency of 351 Hz

This separation was found to be shock induced and prevented a steady mean flow from which the blade vibration analysis could be carried out. These results indicate that the 32.73 IBPA is the least stable IBPA for first natural mode, as observed in experiments, and that the aerodynamic damping is rapidly decreasing with increasing back pressure. It can be easily extrapolated from Figure 14 that further increase in the back pressure would result in a negative aerodynamic damping indicating flutter.

For the back pressure of 16.4 psi, the experiment showed flutter, whereas the analysis predicted the fan to be marginally stable. A possible reason could be the use of an inaccurate operating blade shape. The analysis at the 90 percent speed was performed using the design speed geometry and characteristics. Changes in rotational speed impact the geometry blade shape or more specifically twist distribution. Generating the accurate operating blade shape for 90 percent speed requires iterating between steady aerodynamic analysis and structural analysis, which is an expensive calculation. Therefore, to investigate the effects of changes in blade shape under operating condition, the analysis was carried out on a deformed blade shape obtained by altering the twist distribution along blade span. The blade twist was changed from midspan to tip varying linearly from zero change at midspan to 0.5° change at the tip. The change in twist distribution was such that it increased the incidence of the blade. Structural analysis showed the blade twist change because of changes in centrifugal and aerodynamic loading at the tip to be of this order for the 90 percent speed. The variation in aerodynamic damping with oscillation cycles for the deformed geometry is shown in Figure 15. The changes in twist reduce the damping moving it closer to instability.

Tip-gap and blade natural frequency will also be affected by the rotational speed and can impact the aerodynamic damping calculation. These factors may have contributed to the over prediction of aerodynamic damping. It has been

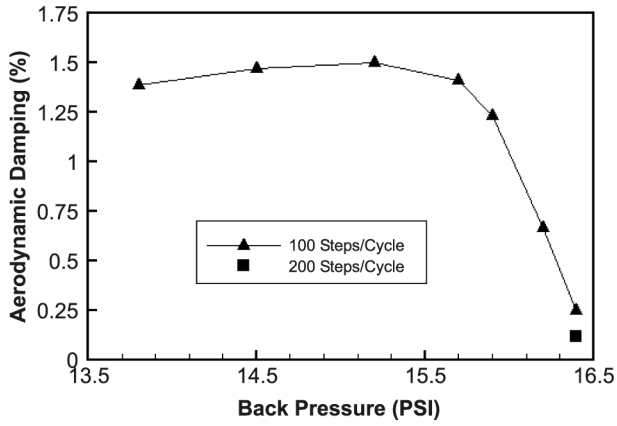

Figure 14.
Variation of aerodynamic damping for 16.4 psi back pressure. Forced vibration in the first natural mode at 351 Hz and 32° IBPA

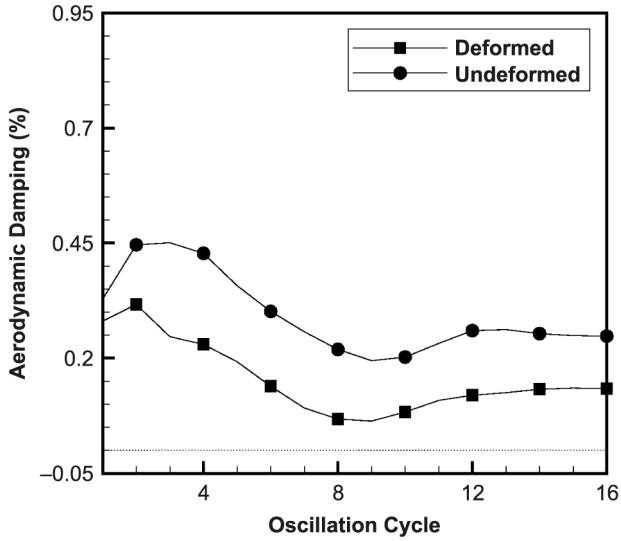

Figure 15.
Effect of change in twist distribution on aerodynamic damping for 16.4 psi back pressure. Forced vibration in the first natural mode at 351 Hz and 32° IBPA at 90 percent speed

reported that tip-gap may have significant impact on stability (Srivastava and Reddy, 1995). The present analysis used a uniform value of tip-gap that is based on measurements made during testing. However, the axial distribution of tip-gap and the accuracy of the measurements are not known. Further, sensitivity analysis did not show a strong influence of natural frequency on the aerodynamic damping.

Analysis was also performed at the second natural vibration mode, which was stable in the experiment. The aerodynamic damping calculated was much higher than those for the first mode, indicating the second mode to be more stable than the first mode. These results clearly show that the analysis successfully calculates the natural mode and IBPA of instability identifying the flutter characteristics of the transonic fan.

Concluding remarks

An aeroelastic analysis program based on the Euler and Navier-Stokes equation has been reported and applied to several turbomachinery components in this study. The calculated unsteady aerodynamic pressure variations are compared with the existing numerical, analytical and experimental results for a helical fan, a turbine cascade and a transonic fan configuration. Good comparisons between analytical and numerical results were found for the helical fan geometry, with the exception being the neighborhood of acoustic resonances. Comparisons with a more challenging case of turbine configuration were also good in general. The trendwise behavior compared very well although the magnitudes did not match accurately. A mild separation was observed in the leading edge area. As the analysis was carried out using

inviscid calculations for this configuration, separated flowfield posed a problem. Comparisons with a linearized viscous analysis further pointed to poor quantitative predictions by TURBO-AE because of the viscous effects. However, the stability analysis results from TURBO-AE compared very well with the linearized viscous analysis indicating a weak influence of viscous effects on stability characteristics for the configuration analyzed.

Calculated variations of aerodynamic damping with back pressure and IBPA is presented for the transonic fan at a condition where flutter occurred during testing. Although a negative aerodynamic damping was not calculated, the analysis yielded qualitatively very good and quantitatively good results. The analysis correctly predicted the mode and IBPA of flutter. Also, the trend for calculated aerodynamic damping clearly indicated a negative aerodynamic damping would result with further increasing the back pressure. Unfortunately, the analysis showed a stalled flowfield would emerge for any further increase of the back pressure. Although flow separation was captured along with vortex shedding, deep blade stall posed a numerical problem.

This two-part paper has detailed an aeroelastic analysis program and its application to turbomachinery blade rows. Part I of the paper highlighted the issues pertaining to phase-lagged analysis techniques and demonstrated the advantages and concerns of various methods that are used. Based on this study it was found that the Fourier-decomposition method was best suited for the work-station environment, whereas the time-shifted method works well for machines with faster input-output devices. Both methods provided equally accurate results. Part II of the paper concentrated on the application of a three-dimensional aeroelastic analysis based on Euler/Navier-Stokes equations, to various turbomachine blade row configurations. It was found that the results obtained for fan configuration compared well with the published results whereas for the turbine configuration the results showed good trendwise behavior. Quantitatively the comparisons were only good to fair. It must be noted here that the analysis for the turbine configuration was carried out using inviscid analysis.

The results presented here required roughly 4-5 days on a SGI Octane per analysis, these computational times are within the realm of engineering analyses. Moreover, these results indicate that the aeroelastic analysis program presented here is accurate and fast enough to be used in engineering applications for aeroelastic analysis of modern turbomachinery components.

References

Bakhle, M.A., Srivastava, R., Keith, T.G. Jr and Stefko, G.L. (1997), "A 3D Euler/Navier-Stokes aeroelastic code for propulsion applications", AIAA Paper No. 97-2749.

Barter, J.W., Vitt, P.H. and Chen, J.P. (2000), "Interaction effects in a transonic turbine stage", ASME paper 2000-GT-0376, May 2000.

Breard, C., Vahadati, M., Sayma, A.I. and Imregun, M. (2000), "An integrated time-domain aeroelasticity model for the prediction of fan forced response due to inlet distortion", ASME Paper 2000-GT-0373.

Carta, F.O. (1967), "Coupled blade-disk-shroud flutter instabilities in turbojet engine rotors", *Journal of Engineering for Power*, pp. 419-26.

Chen, J.P. (1991), "Unsteady three-dimensional thin-layer Navier-Stokes solutions for turbomachinery in transonic flow", PhD dissertation, Mississippi State University.

Chen, J.P. and Barter, J. (1998), "Comparison of time-accurate calculations for the unsteady interaction in turbomachinery stage", AIAA Paper No. 98-3292.

Clark, W.S. (1998), "Investigation of unsteady viscous flows in turbomachinery using a linearized Navier-Stokes analysis", PhD dissertation, Duke University.

Clark, W.S. and Hall, K.C. (2000), "A time-linearized Navier-Stokes analysis of stall flutter", *Journal of Turbomachinery*, Vol. 122 No. 3, pp. 467-76.

Fite, B.E. (2001), "Aerodynamic overview of the NASA/Honeywell quiet high speed fan test", *Presented at the Noise Reduction/QAT Technical Working Group Meeting*, April 2001, East Hartford, CT.

Gerolymos, G.A. (1992), "Coupled 3D aeroelastic stability analysis of bladed disks", ASME Paper No. 92-GT-171.

Gerolymos, G.A. and Vallet, I. (1994), "Validation of 3D Euler methods for vibrating cascade aerodynamics", ASME Paper 94-GT-294.

Giles, M. and Haimes, R. (1991), "Validation of a numerical method for unsteady flow calculations", ASME Paper 91-GT-271.

He, L. (1989), "An Euler solution for unsteady flows around oscillating blades", *ASME Journal of Turbomachinery*, Vol. 112 No. 4, pp. 714-22.

He, L. and Denton, J.D. (1994), "Three-dimensional time marching inviscid and viscous solutions for unsteady flows around vibrating blades", *ASME Journal of Turbomachinery*, Vol. 116, pp. 469-76.

Janus, J.M. (1989), "Advanced 3D CFD algorithm for turbomachinery", PhD dissertation, Mississippi State University, Mississippi.

Lane, F. and Friedman, M. (1958), "Theoretical investigation of subsonic oscillating blade-row aerodynamics", NACA TN 4136.

Marshall, J.G., Denton, J., Xu, L. and Chew, J.W. (2000), "Prediction of low engine order inlet distortion driven resonance in a low aspect ratio fan", ASME Paper 2000-GT-0374.

Montgomery, M.D. and Verdon, J.M. (1997), "A three-dimensional linearized unsteady Euler analysis for turbomachinery blade rows", NASA CR-4770.

Rothrock, M.D., Jay, R.L. and Riffel, R.E. (1981), "Time variant aerodynamics of high-turning blade elements", ASME Paper 81-GT-123.

Shih, T-H., Liou, W.W., Shabbir, A., Yang, Z. and Zhu, J. (1995), "A New k-ε Eddy viscosity model for high Reynolds number turbulent flows", *International Journal of Computers and Fluids*, Vol. 24 No. 3, pp. 227-38.

Siden, L.D.G. (1991), "Numerical simulation of unsteady viscous compressible flows applied to a blade flutter analysis", ASME Paper No. 91-GT-203.

Smith, S.N. (1972), "Discrete frequency sound generation in axial flow turbomachines", R&M 3709, British Aeronautical Research Council, London, England, UK.

Srivastava, R. and Reddy, T.S.R. (1995), "Aeroelastic analysis of ducted rotors", *Proceedings of International Symposium on Computational Fluid Dynamics in Aeropropulsion*, November 1995, Vol. 49, San Francisco, pp. 1-9.

Srivastava, R. and Reddy, T.S.R. (1999), "Comparative study of coupled-mode flutter-analysis methods for fan configurations", *Journal of Propulsion and Power*, Vol. 15 No. 3, pp. 447-53.

Srivastava, R., Bakhle, M.A., Keith, T.G. Jr and Stefko, G.L. (2004), "Aeroelastic analysis of turbomachinery. Part I – phase lagged boundary condition methods", *International Journal of Numerical Methods for Head & Fluid Flow*, Vol. 14 No. 3.

Verdon, J.M. (1989), "The unsteady flow in the far field of an isolated blade row", *Journal of Fluids and Structures*, Vol. 3 No. 2, pp. 123-49.

Verdon, J.M. (1993), "Unsteady aerodynamic methods for turbomachinery aeroelastic and aeroacoustic applications", *AIAA Journal*, Vol. 31 No. 2, pp. 235-50.

Williams, M.H., Cho, J. and Dalton, W.N. (1991), "Unsteady aerodynamic analysis of ducted fans", *Journal of Propulsion and Power*, Vol. 7 No. 5, pp. 800-4.